

## AN EXPERIMENTAL STUDY ON THE FORMABILITY OF A VIBRATION DAMPING SANDWICH SHEET (BONDAL)

Abdolvahed KAMI<sup>1</sup>, Bijan MOLLAEI DARIANI<sup>2</sup>, Dan Sorin COMSA<sup>3</sup>, Dorel BANABIC<sup>3</sup>,  
Ali SADOUGH VANINI<sup>2</sup>, Mathias LIEWALD<sup>4</sup>

<sup>1</sup> Semnan University, Mechanical Engineering Department, Semnan, Iran

<sup>2</sup> Amirkabir University of Technology, Mechanical Engineering Department, Tehran, Iran

<sup>3</sup> Technical University of Cluj-Napoca, CERTETA Research Centre, Cluj-Napoca, Romania

<sup>4</sup> Institute for Metal Forming Technology (IFU) – Holzgartenstr. 17, 70174 Stuttgart, Germany

Corresponding author: E-mail: banabic@tcm.utcluj.ro

**Abstract.** Bondal is the denomination of a vibration damping sandwich sheet, which is mainly used in automotive industry for sound and vibration damping. In this paper, the formability of this sheet was investigated by conducting different types of experiments such as uniaxial tensile, hydraulic bulge, Nakazima and T-peel tests. Furthermore, SEM analyses have been performed to assess the bonding strength of layers and possible delamination due to deformation. The obtained results include the uniaxial tensile curves of the Bondal sheet and its components, the forming limit diagram (FLD) of the Bondal sheet, bulging limit strains and bulging height at the onset of fracture, T-peel test force curves and so on.

**Key words:** forming limit diagram, FLD, Bondal sandwich sheet, Bulge test, vibration damping.

### 1. INTRODUCTION

In looking for materials with properties such as light weight, high strength to weight ratio, sound insulation, vibration damping, good formability and so on, one technological solution was the introduction of the sandwich sheets. Until now, different types of sandwich sheets have been developed. An important category of them is the metal/polymer/metal (MPM) sandwich sheets. Hylite [1], Bondal [2] and Litecor [3] are examples of commercial MPM sandwich sheets, specially developed for automotive industry.

Bondal is a vibration-damping sandwich sheet with a viscoelastic core and two outer steel skin sheets [2]. It offers high structure-borne sound insulation and good airborne sound damping properties and can be used to great effect wherever steel components are subjected to vibrations resulting in structure-borne sound [4]. Some information about the real applications and finite element simulation of the Bondal sheet have been presented in references [5, 6]. However, a few works have been published about the formability and the behavior of the sheet during deformation. Engel and Buhl [7, 8] performed tensile shear test at different velocities and overlapping widths. Also, they analyzed the displacement of metallic layers and their delamination during bending. Furthermore, Engel and Buhl [9] provided optimum conditions for conducting bending without delamination. The simulation of the Bondal sheet during bending and deep drawing has been done numerically [10, 11], which is actually the assessment of the applicability of solid-shell elements in the sheet forming processes.

From the above literature survey, one may conclude that to assess the formability of the Bondal sheet, more comprehensive investigations are required to be performed. Consequently, in this paper, the formability of this sheet was investigated by conducting tensile, hydraulic bulge, Nakazima and T-peel tests. Furthermore, SEM analyses have been performed to assess the bonding strength of layers and possible delamination due to deformation.

## 2. UNIAXIAL TENSILE TESTS

Bondal is a three layer sandwich sheet with the thickness of 1.25 mm. It has two DC06 steel skin sheets with the thickness of 0.6 mm and a viscoelastic core layer with the thickness of 0.05 mm. To obtain the mechanical properties of the sandwich sheet and its constitutive layers, the uniaxial tensile tests have been carried out on the sandwich sheet and its metallic layers. The mechanical properties of the core layer have been calculated in a subsequent stage, using the equilibrium condition in the tensile direction.

The tensile experiments have been conducted on a Zwick tensile testing machine with 15 tons capacity. The experiments have been performed on specimens cut at  $0^\circ$ ,  $45^\circ$  and  $90^\circ$  with respect to the rolling direction and with the rate of 0.001 1/s (according to the DIN EN 10002-1:2001-12 standard [12]). In all cases, rectangular specimens with the dimensions 200 mm  $\times$  20 mm  $\times$  1 mm have been used. In each direction, the tests have been repeated five times. Fig. 1 illustrates the true stress-true strain curve of the Bondal sheet in the rolling direction. A summary of the mechanical properties of the Bondal and DC06 skin sheets, obtained from the tensile tests, is given in Table 1 and Table 2, respectively. In these tables,  $K$  and  $n$  are the hardening strength and hardening exponent of the Holloman's hardening law [13], respectively. As one may notice from Table 1 and Table 2, the mechanical properties of the Bondal and DC06 skin sheets are very close to each other. This is due to the fact that the core layer has a small thickness value, 0.05 mm. So, this layer is not able to significantly affect the tensile properties of the Bondal sheet.

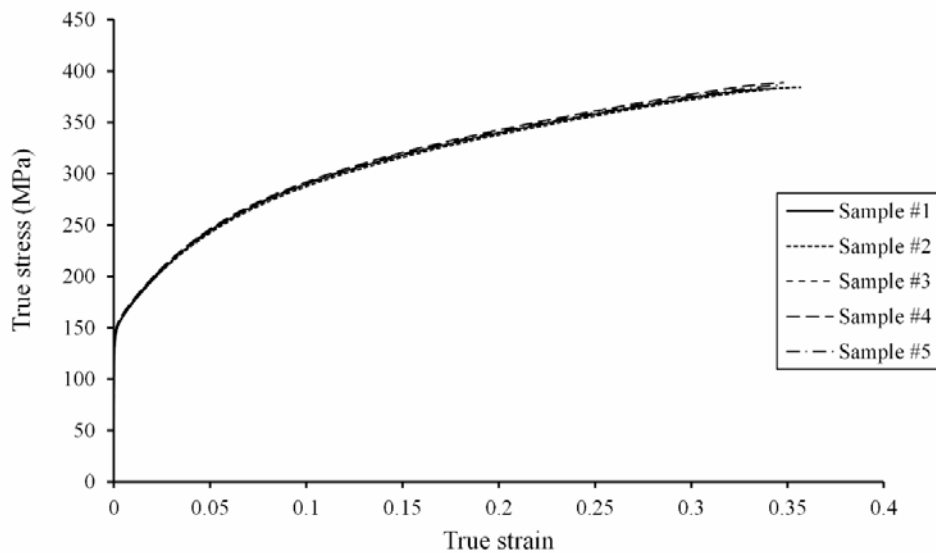


Fig. 1 – The true stress-true strain curves of the Bondal sheet in the rolling direction ( $0^\circ$ ).

Table 1

Mechanical properties of the Bondal sheet (1.25 mm thickness)

Orientation	Lankford coefficient, $r$	Yield stress, [MPa]	Tensile strength, [MPa]	$K$ [MPa]	$n$
$0^\circ$	2.020	152	270	487	0.241
$45^\circ$	1.741	159	272	489	0.235
$90^\circ$	2.510	154	264	477	0.237

Table 2

Mechanical properties of the DC06 skin sheet (0.6 mm thickness)

Orientation	Lankford coefficient, $r$	Yield stress, [MPa]	Tensile strength, [MPa]	$K$ [MPa]	$n$
$0^\circ$	2.027	152	279	504	0.241
$45^\circ$	1.751	160	286	515	0.238
$90^\circ$	2.467	156	274	492	0.235

The stress-strain curve of the core layer can be calculated by writing the force equilibrium in each tension direction. To do this, the gauge region in the current configuration of a tensile test has been considered for the specimens cut from the sandwich and DC06 skin sheets (see Fig. 2). The skin and core layers of the sandwich gauge are assumed to preserve their volumes during the tensile test:

$$V_{skin} = {}^{(0)}V_{skin}, \quad V_{core} = {}^{(0)}V_{core}. \quad (1)$$

These parameters have been defined in Table 3. With the help of the relationships given in Table 3, it follows from Equation (1) that:

$$A_{skin} = {}^{(0)}A_{skin} \exp(-\varepsilon), \quad A_{core} = {}^{(0)}A_{core} \exp(-\varepsilon), \quad A = {}^{(0)}A \exp(-\varepsilon), \quad (2)$$

where

$$\varepsilon = \varepsilon_{skin} = \varepsilon_{core} = \ln \frac{l}{{}^{(0)}l} \quad (3)$$

is the axial logarithmic strain of the gauge region (its value is the same for the skin and core layers).

The tensile force carried by the sandwich gauge can be decomposed into skin and core contributions,

$$F = 2F_{skin} + F_{core}, \quad (4)$$

or, equivalently,

$$\sigma A = 2\sigma_{skin} A_{skin} + \sigma_{core} A_{core}, \quad (5)$$

where  $\sigma$ ,  $\sigma_{skin}$  and  $\sigma_{core}$  denote the current value of the tensile stress acting on the cross section of the sandwich sheet, skin layer and core layer, respectively. Equation (2) and the relationships given in Table 3 allow rewriting Equation (5) in the form

$$\begin{aligned} \sigma_{core} &= \sigma \frac{A}{A_{core}} - 2\sigma_{skin} \frac{A_{skin}}{A_{core}} = \sigma \frac{{}^{(0)}A}{{}^{(0)}A_{core}} - 2\sigma_{skin} \frac{{}^{(0)}A_{skin}}{{}^{(0)}A_{core}} \\ &= \sigma \frac{2{}^{(0)}s_{skin} + {}^{(0)}s_{core}}{{}^{(0)}s_{core}} - 2\sigma_{skin} \frac{{}^{(0)}s_{skin}}{{}^{(0)}s_{core}} = 2(\sigma - \sigma_{skin}) \frac{{}^{(0)}s_{skin}}{{}^{(0)}s_{core}} + \sigma. \end{aligned} \quad (6)$$

One assumes that tensile tests have been performed on specimens cut from the sandwich sheet, as well as from the skin layer. The results of these experiments consist in tabular representations of the stress vs. strain curves  $\left\{ \left[ \varepsilon^{(i)}, \sigma^{(i)} \right] \mid i = 1, \dots, N \right\}$  for the sandwich sheet, and  $\left\{ \left[ \varepsilon^{(i)}, \sigma_{skin}^{(i)} \right] \mid i = 1, \dots, N \right\}$  for the skin layer.

Both representations should refer to the same discrete set of axial logarithmic strains  $\left\{ \varepsilon^{(i)} \mid i = 1, \dots, N \right\}$ .

Equation (6) can be used to compute the tensile stress acting on the cross section of the core layer for each value  $\left\{ \varepsilon^{(i)} \mid i = 1, \dots, N \right\}$ :

$$\sigma_{core}^{(i)} = 2 \left[ \sigma^{(i)} - \sigma_{skin}^{(i)} \right] \frac{{}^{(0)}s_{skin}}{{}^{(0)}s_{core}} + \sigma^{(i)}, \quad i = 1, \dots, N. \quad (7)$$

A tabular representation  $\left\{ \left[ \varepsilon^{(i)}, \sigma_{core}^{(i)} \right] \mid i = 1, \dots, N \right\}$  is obtained in this way.

Because of the fact that  $\left\{ \varepsilon^{(i)} \mid i = 1, \dots, N \right\}$  are strains highly dominated by their plastic part, tabular representations of the hardening curves associated to the sandwich sheet and skin layer can be used instead of  $\left\{ \left[ \varepsilon^{(i)}, \sigma^{(i)} \right] \mid i = 1, \dots, N \right\}$  and  $\left\{ \left[ \varepsilon^{(i)}, \sigma_{skin}^{(i)} \right] \mid i = 1, \dots, N \right\}$ . Of course, in such a case, a tabular representation of

the core hardening curve  $\left\{ \left[ \varepsilon^{(i)}, \sigma_{core}^{(i)} \right] \mid i = 1, \dots, N \right\}$  is obtained from Equation (7). The set of discrete values  $\left\{ \left[ \varepsilon^{(i)}, \sigma_{core}^{(i)} \right] \mid i = 1, \dots, N \right\}$  obtained in this way can be used for calibrating an empirical hardening law associated to the core layer.

By employing Equation (7), the stress vs strain curve of the core layer has been obtained as Fig. 2 and its hardening law was calculated as  $\sigma_{core} = 79\bar{\varepsilon}^{0.241}$ , where  $\bar{\varepsilon}$  is the equivalent plastic strain.

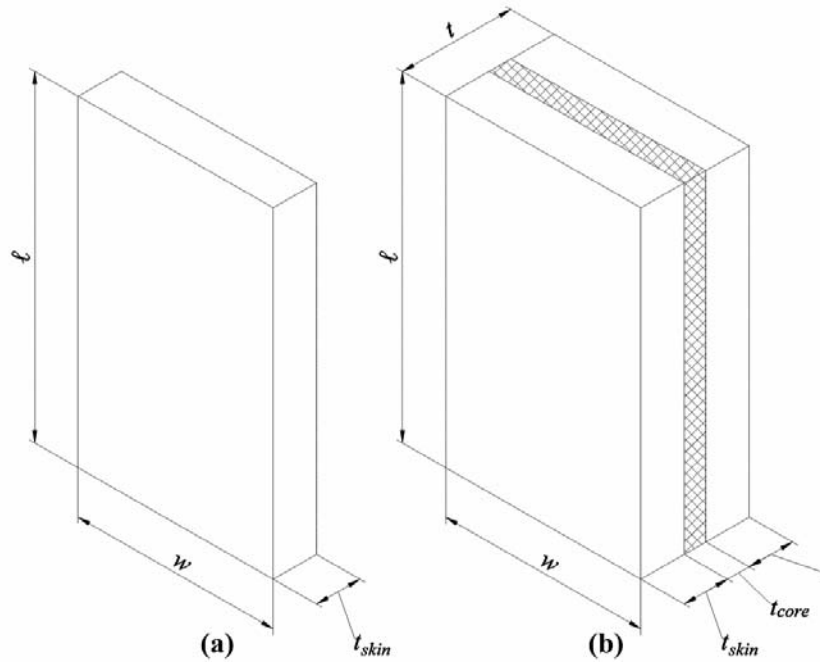


Fig. 2 – Dimensions of the gauge region in the current configuration of a tensile test:  
a) specimen cut from the DC06 skin sheet and b) specimen cut from the Bondal sandwich sheet.

Table 3

Dimensional parameters of the gauge region  
corresponding to the current configuration of the tensile test (see Fig. 2)

$l$	gauge length
$w$	gauge width
$s_{skin}$	thickness of the skin gauge
$s_{core}$	thickness of the core gauge
$s = 2s_{skin} + s_{core}$	thickness of the sandwich gauge
$A_{skin} = ws_{skin}$	cross-sectional area of the skin gauge
$A_{core} = ws_{core}$	cross-sectional area of the core gauge
$A = ws = w(2s_{skin} + s_{core}) = 2A_{skin} + A_{core}$	cross-sectional area of the sandwich gauge
$V_{skin} = lA_{skin}$	volume of the skin gauge
$V_{core} = lA_{core}$	volume of the core gauge
$V = lA = l(2A_{skin} + A_{core}) = 2V_{skin} + V_{core}$	volume of the sandwich gauge
Note: When preceded by the “(0)” superscript (for example, ${}^{(0)}s$ ), the symbols listed above denote dimensional parameters corresponding to the initial configuration of the gauge region.	

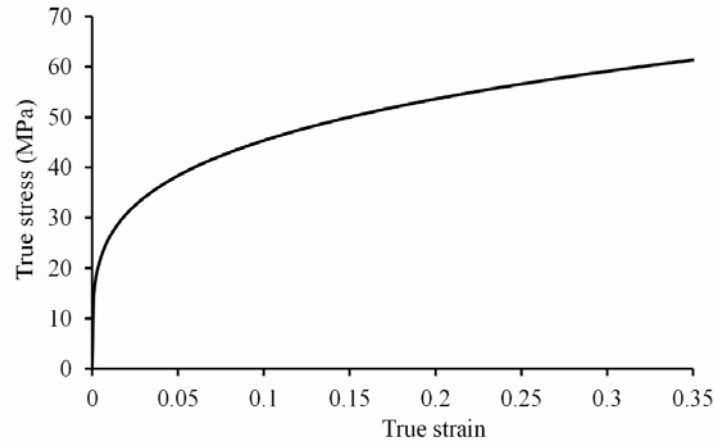


Fig. 3 – The true stress-true strain curve of the core layer obtained by the volume constancy assumption and force equilibrium in the rolling direction.

### 3. FORMING LIMIT DIAGRAM OF THE BONDAL SHEET

Forming limit diagram (FLD) is a common tool for the determination of strain limits in sheet metal forming. It defines the major,  $\varepsilon_1$  and minor  $\varepsilon_2$ , limit strains at the surface of the sheet metal. Different approaches have been introduced for the experimental determination of FLD [14]. A common approach is the Nakazima test, which is a set of hemispherical punch stretching tests that induce different strain evolutions in the central area of the specimen [14]. Each strain path is characterized by the ratio of minor and major principal surface strain. Different loading conditions ranging from uniaxial traction to balanced-biaxial traction can be obtained by modifying the width of the specimen shaft. These loads cover both the left and right branches of a forming limit curve.

Because of some limitations, the FLD has been determined only for the Bondal sandwich sheet. Based on the explained methodology in the ISO 12004-2 standard [15], six discrete load states have been considered and the limit strains associated to each of these states have been calculated by averaging the results of three repetitions of the Nakajima tests. The values of the shaft width adopted by the authors are 30 (uniaxial traction), 90, 110, 130, 140 and 190 mm (balanced-biaxial traction), the last of them corresponding to a fully circular specimen. To eliminate the delamination of layers and having good edge quality, the water-jet process has been used to cut the specimens. Figure 4 shows the six Nakazima test samples after conducting the test.



Fig. 4 – The six Nakazima test samples with three repetitions.

Figure 5 shows the Erichsen testing machine (model 142–20) and the ARAMIS strain-measurement system used in the experiments. Before each Nakajima test, a stochastic cloud of black spots has been sprayed onto the upper surface of the specimen. The limit strains have been determined with the ARAMIS software by applying the position-dependent methodology recommended in the ISO 12004-2 standard [15]. The FLD obtained in this manner is shown in Fig. 6.



Fig. 5 – Erichsen testing machine (model 142–20) and ARAMIS strain-measurement system used for the experimental determination of the forming limit curve.

From Fig. 6 one may notice that the Nakajima test on the circular specimen results in the  $\varepsilon_1 = 0.436$  and  $\varepsilon_2 = 0.285$  values of the limit strains, which is far from the equi-biaxial point. This might be the effect of the friction between the specimen and the punch. A better equi-biaxial point has been obtained by conducting the hydraulic bulge test (see the extreme right point in Fig. 6). This point has the  $\varepsilon_1 = 0.403$  and  $\varepsilon_2 = 0.378$  values of the limit strains, which are very close to the equi-biaxial state. The hydraulic bulge test has been carried out on a circular specimen with the diameter of 185 mm and it has been repeated three times. Figure 7 depicts the three samples of the bulge test of the Bondal sheet.

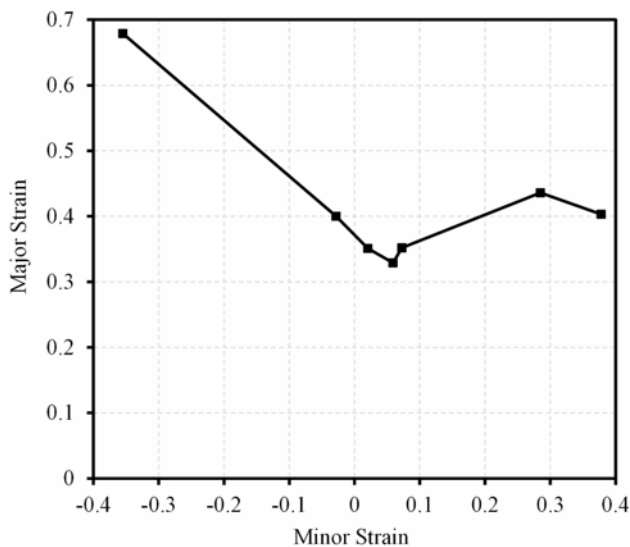


Fig. 6 – Experimental FLD of the Bondal sandwich sheet (1.25 mm thickness).



Fig. 7 – Hydraulic bulge test samples of Bondal sheet.

#### 4. DELAMINATION OF THE LAYERS

An important aspect in using the adhesive bonded sandwich sheets in metal forming operations is the delamination of the layers. Two major delamination modes exist: the shear load delamination and the tensile load delamination. During deformation one delamination mode or both of them may become active and may result in delamination of the layers.

In case of the Bondal sandwich sheet, useful data about the bonding strength of the layers in the shear loading mode have been provided by Engel and Buhl [7, 9]. In this research, the bonding strength of the Bondal sheet layers in the tensile loading mode has been examined. So, T-peel tests have been performed based on the instructions of ASTM D1876 [16]. The dimensions of the T-peel test specimens are illustrated in Fig. 8. The test has been conducted using a 15 ton Zwick tensile testing machine. In Fig. 9, one T-peel test specimen is shown during the test. It has been observed that the core layer separates from one skin layer and remains bonded to the other skin layer.

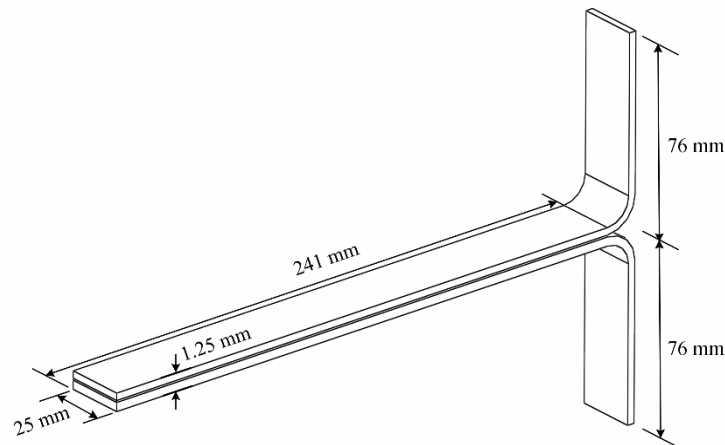


Fig. 8 – Dimensions of the Bondal T-peel test sample according to ASTM D1876 [16].



Fig. 9 – The T-peel test performed on a Bondal sandwich sheet.

The T-peel test has been carried out on six test specimens. The force-travel curve of these test specimens has been almost the same. The full separation of the layers has occurred after 360 mm travel the tensile test machine grips. After about 100 mm travel of the grips the force remains almost constant at 13 N. Figure 10 depicts the average force-travel curve along the first 30 mm travel of the grips. This figure shows that the maximum force value is 53.7 N which occurs at about 1.03 mm travel of the machine grip.

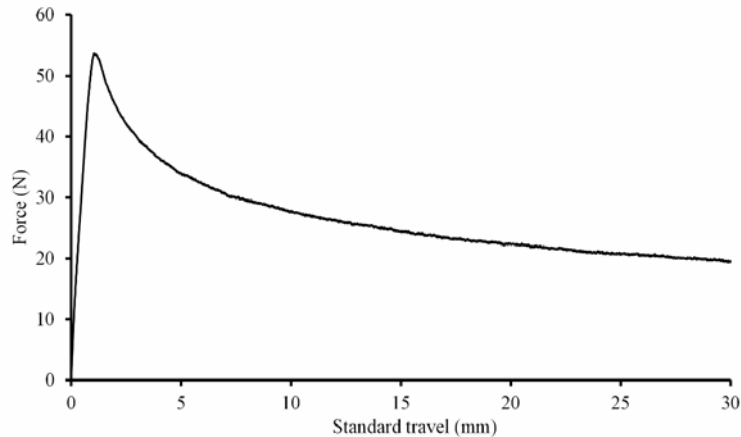


Fig. 10 – The average force-travel curve of the T-peel test.

The possible delamination of the layers has been studied by SEM analysis on the as received and also the deformed tensile test specimens. Figure 11 illustrates the SEM images taken from the cross-section of a deformed tensile specimen. The SEM images of the as received Bondal sheet are not included here. The SEM analyses show an intimate adherence of the core to the metallic skins both in the case of the as received material and the fractured specimen (see Fig. 11). The fracture tip of specimen (see Fig. 11a) is the only place where a separation can be observed, but this seems to be the consequence of the fact that the fracture surfaces of the upper and lower skins are slightly shifted. Furthermore, it seems that the core layer deformation has continued after the fracture of the metallic skins (see the fracture zone in Fig. 11a). So, one may conclude that during the deformation of the Bondal sheet, the metallic skins are the first layers to fail.

## 5. CONCLUSIONS

In this paper, the mechanical properties of the Bondal sandwich sheet have been determined by conducting tensile, Nakazima, hydraulic bulge and T-peel tests. The results of this study provide useful information for the application of the Bondal sheet in metal forming operations. The summary of the results is as follows:

- The tensile properties of the Bondal sandwich sheet and its DC06 skin sheets are very close to each other.
- The FLD of the Bondal sheet indicates that the sheet has a very good formability. The full FLD of the sheet was determined by conducting both Nakazima and hydraulic bulge tests.
- The maximum average peeling force value was found equal to 53.7 N, which occurred at about 1.03 mm travel of the test machine grip.
- The SEM analyses showed an intimate adherence of the core to the metallic skins both in the case of the as received material and the fractured specimen. Furthermore, the SEM images reveal that during the deformation of the Bondal sheet, the fracture of the viscoelastic core layer occurs after the fracture of the metallic skin.

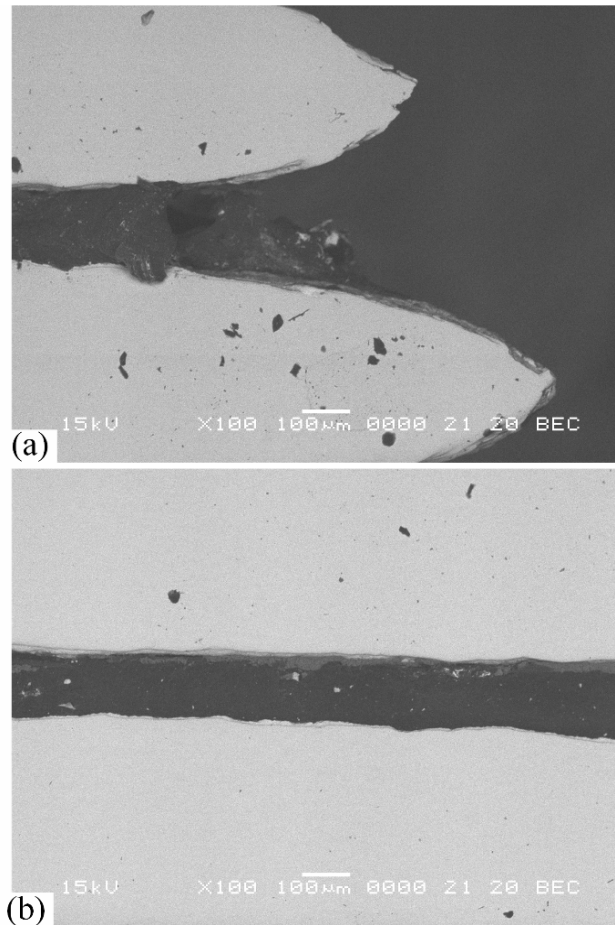


Fig. 11 – The composition SEM images from the section of tensile specimens after fracture with  $\times 100$  magnification: a) the fracture zone; b) a farther location with 1 mm distance from the fracture zone.

## ACKNOWLEDGEMENTS

The authors would like to thank the ThyssenKrupp Steel Europe AG for providing the Bondal sheet samples. The authors also thank Dr. Ioan Nicodim for his kind help in conducting the experiments.

## REFERENCES

1. BURCHITZ I., BOESENKOOL R., ZWAAG S.V.D., TASSOUL M., *Highlights of designing with Hylite – a new material concept*, *Materials & Design*, **26**, 4, pp. 271–279, 2005.
2. THYSSENKRUPP STAHL A., *Data sheet Bondal®: Composite material with structure and airborne sound damping properties*, Bochum, 2012.
3. THYSSENKRUPP STEEL, A., *Litecor: the intelligent solution for cost-effective lightweight design*, Germany, Duisburg, 2012.
4. CENTER T.S.S., *BONDAL®*, <http://www.thyssenkrupp-stahl-service-center.com/en/583.html>
5. FILTHAUT C., MÜLLER R., *Schwingungsdämpfendes verbundblech – Schalldämpfung ab werk*, *JOT Journal für Oberflächentechnik*, **40**, 4, pp. 42–45, 2000.
6. PIERONEK D., BÖGER T., RÖTTGER R., *Modeling approach for steel sandwich materials in automotive crash simulations*, 2012.
7. ENGEL B., BUHL J., *Metal forming of vibration-damping composite sheets*, *Steel Research International*, **82**, 6, pp. 626–631, 2011.
8. ENGEL B., BUHL J., *Forming of sandwich sheets considering changing damping properties, metal forming-process, tools, design*, in *Metal Forming-Process, Tools, Design*, D.M. Kazeminezhad (Ed.), InTech, 2012.
9. ENGEL B., BUHL J., HEFTRICH C., *Modelling and Optimization of Lightweight-Sandwich-Sheets with an Adhesive Interlayer for the Forming Process Die Bending*, *Procedia CIRP*, **18**, pp. 168–173, 2014.

10. HARNAU M., *Finite volumen-schalenelemente für große deformationen und kontakt*, PhD, Institut für Mechanik, Universität Karlsruhe, 2004.
11. HARNAU M., SCHWEIZERHOF K., *Artificial kinematics and simple stabilization of solid-shell elements occurring in highly constrained situations and applications in composite sheet forming simulation*, *Finite Elements in Analysis and Design*, **42**, 12, pp. 1097–1111, 2006.
12. Beuth Verlag GmbH, *Metallic materials-Tensile testing. Part 1: Method of testing at ambient temperature*, DIN EN 10002-1:2001-12, English version, Berlin, 2001.
13. HOLLOMON J. H., *Tensile deformation*, *AIME TRANS*, **12**, 4, pp. 1–22, 1945.
14. BANABIC D., *Formability of sheet metals*, in *Sheet Metal Forming Processes*, D. Banabic (Ed.), Heidelberg: Springer, 2010, pp. 141–211.
15. INTERNATIONAL ORGANIZATION for STANDARDIZATION, *Metallic Materials-sheet and Strip-Determination of Forming Limit Curves. Part 2: Determination of Forming Limit Curves in the Laboratory, ISO 12004-2*, Geneva, Switzerland, 2008.
16. ASTM International, *Standard test method for peel resistance of adhesives (T-Peel test)*, ASTM D1876-00, West Conshohocken, PA, 2001.

*Received April 14, 2016*